# High-Resolution Imaging of the Intramolecular Structure of Indomethacin–Carrying Dendrimers by Scanning Tunneling Microscopy

**Christopher J. Fleming, Nai-Ning Yin, Shawn L. Riechers, Gabriel Chu, and Gang-yu Liu***

Department of Chemistry, University of California, Davis, California 95616, United States

**ABSTRACT** Dendrimers have shown great potential in drug delivery because of their enhancement of drug solubility in aqueous media, leading to an increase in *in vivo* circulation and efficacy to targets. The structure of drug–dendrimer complexes however, is not well-known owing to the difficulties associated with visualizing individual drug molecules attached to dendrimers. Scanning tunneling microscopy (STM) enables visualization of dendrimer intramolecular structures using our approach of metal ion tagging. This work extends the approach to reveal the hierarchical structure of indomethacin-loaded poly(amidoamine) hydroxyl-terminated dendrimers. STM imaging provides structural information such as their height, lateral dimensions, and volume. High-resolution STM images enable the identification and count of individual indomethacin molecules bound to the anterior of dendrimers. Removal of drug molecules by the STM tip allows the calculation of individual drug-dendrimer binding energy, which is consistent with 1–3 hydrogen bonds. These investigations provide new insight into the hierarchical structure and nature of indomethacin–dendrimer interactions and deepen our understanding of the stability and pharmacokinetic behavior of dendrimer-based drug delivery vehicles.

**KEYWORDS:** self-assembled monolayer · dendrimers · hierarchical structure · drug delivery · STM · nanocarrier

Dendrimers show great promise in drug delivery[1–4] as they increase solubility and *in vivo* compatibility of drug molecules such as nonsteroidal anti-inflammatory drugs (NSAIDs).[5–9] Among NSAIDs tested, most of them such as ketoprofen, aspirin, and indomethacin revealed better pharmacokinetic performance when delivered by poly(amidoamine) (PAMAM) dendrimers.[10–12] Despite the lack of direct observation, this enhancement was rationalized by the molecular level interactions between drug and dendrimers.[13–16] The PAMAM system contains successive iterations of amidoamine chains which branch from tertiary amines and are capped by functionalized termini.[17] NSAIDs such as indomethacin could attach to the hydroxyl-termini or the intramolecular amines *via* hydrogen bonds,[13–16] resulting in an enhancement factor up to 3.25 times for reported rat edema models.[6] Similar solubility and performance enhancement has also been found in ketoprofen–PAMAM[7] and ibuprofen–PAMAM dendrimer[11] systems.

Further enhancement of solubility and delivery performance could be attained by increasing the load (*i.e.*, higher number of drug molecules per dendrimer) and attaining designed drug–dendrimer interactions to achieve stability and release. These desired interactions could benefit from the experimental measurements of load and drug–dendrimer interactions. While structural information of drug molecules on the exterior and interior of dendrimers have been postulated through Molecular Dynamics simulations,[13,16,18] direct evidence from experiments are still lacking due to difficulties in visualizing intramolecular structures of drug carrying dendrimers.

Scanning tunneling microscopy (STM) is known to provide the highest spatial resolution imaging, reaching submolecular and even atomic resolution for conductive and semiconductive systems.[19–25] Using metal ion tagging, our previous studies showed that STM enabled the visualization of intramolecular features of PAMAM dendrimers such as their hydroxyl termini.[21] In this investigation, we extended this approach successfully to indomethacin carrying dendrimers. STM investigations enable imaging of the hierarchical structure of the PAMAMs and indomethacin molecules, and determination of the strength of indomethacin–PAMAM interactions. The insights provided in this study shall benefit the design of more effective dendrimers and optimization of the delivery performance.

* Address correspondence to liu@chem.ucdavis.edu.

Received for review August 18, 2010 and accepted January 31, 2011.

**Published online February 15, 2011**
10.1021/nn103609b

## RESULTS AND DISCUSSION

**Uploading of Indomethacin Resulted in Increased Dendrimer Volume.** STM imaging reveals that G4 PAMAM−OH−$(Pt^{2+})_n$−$(Indo)_m$ dendrimers are taller than the base G4 dendrimers. Figure 1A is a 18 × 18 $nm^2$ STM topograph of G4 PAMAM−OH−$(Pt^{2+})_n$−$(Indo)_m$ dendrimers immobilized on Au(111). The inset in Figure 1A is a 60 × 60 $nm^2$ STM topographic image showing the high surface coverage. The bright protrusions correspond to individual G4 PAMAM−OH−$(Pt^{2+})_n$−$(Indo)_m$ dendrimer molecules. The STM apparent height, or $h_{APP}$, is obtained by measuring the height from the lowest point in the immediate surrounding matrix to the top of the dendrimer. In cursor profiles 1 and 2, the indomethacin-loaded dendrimer is colored dark blue for differentiation from the surrounding matrix which is shaded gray. These cursors indicate that dendrimers loaded with indomethacin adopt an elliptical dome shape similar to the base dendrimers reported previously.[17,21,26] The $h_{APP}$ in cursor profiles 1 and 2 is 0.50 and 0.57 nm, respectively. Figure 1B is a 18 × 18 $nm^2$ STM topograph of G4 PAMAM−OH−$(Pt^{2+})_n$ dendrimers immobilized on Au(111) obtained at the same *I*−*V* set point as Figure 1A. The bright, spherical protrusions correspond to individual, surface-bound dendrimers. The inset in Figure 1B, a 60 × 60 $nm^2$ STM topograph, shows similar surface coverage to the inset in Figure 1A. Cursor profiles 3 and 4 provide the $h_{APP}$ of the chosen G4 dendrimers, 0.40 and 0.46 nm, respectively. The $\Delta h_{APP}$ between the selected G4 PAMAM−OH−$(Pt^{2+})_n$−$(Indo)_m$ and G4 PAMAM−OH−$(Pt^{2+})_n$ dendrimers in Figure 1 is 0.10 nm. Among the 102 dendrimers we compared, drug-loaded G4 dendrimers appear 0.09 ± 0.02 nm taller than the dendrimers themselves.

Because the STM topographic contrast depends on the physical height as well as local density of states (LDOS),[27−29] AFM was used to calibrate $h_{APP}$ to the true height, $h_{REAL}$, using the same sample immediately after the STM experiments. Figure 2A is a AFM topographic image (300 × 300 $nm^2$) of the same surface as in Figure 1A. To measure the height accurately, the dendrimers in the central 500 × 500 $nm^2$ area (insert in Figure 2A) were removed to expose the Au surface. The height of G4 PAMAM−OH−$(Pt^{2+})_n$−$(Indo)_m$ dendrimers, $h_{REAL}$ = 3.4 ± 0.7 nm, was obtained by averaging the height difference between the Au substrate and top of those dendrimer in the surrounding area.

Similar measurements were carried out for G3 PAMAM−OH−$(Pt^{2+})_n$−$(Indo)_m$ and G5 PAMAM−OH−$(Pt^{2+})_n$−$(Indo)_m$. These three systems follow a linear relationship of $h_{REAL} = 2.45h_{APP} + 2.21$ (nm). This trend is anticipated as the three indomethacin−dendrimer complexes are the same class of system in terms of structure and conductivity. As a comparison to the control systems, for example, bare G4, Figure 2B and cursor 2 reveal a typical height of $h_{REAL}$ = 2.5 ± 0.3 nm,

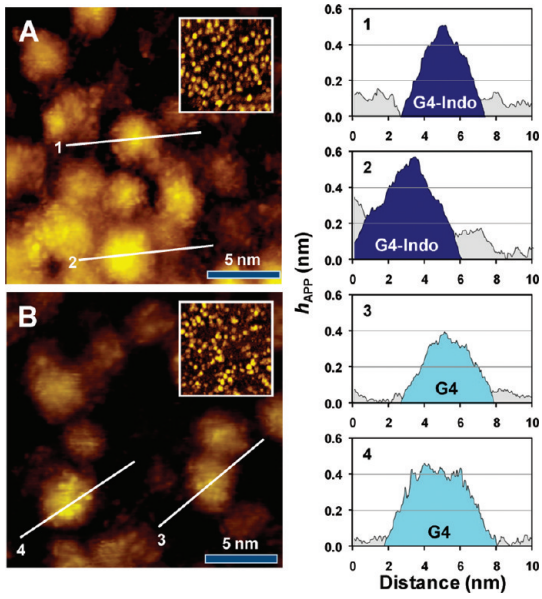


**Figure 1. STM images of indomethacin-loaded *vs* unloaded dendrimers under the same imaging condition: 0.30 V and 15 pA. (A) An 18 × 18 $nm^2$ of topographical image of G4 PAMAM−OH−$(Pt^{2+})_n$−$(Indo)_m$ dendrimers immobilized on a Au(111) film. (B) An 18 × 18 $nm^2$ scan of G4 PAMAM−OH−$(Pt^{2+})_n$ dendrimers on gold. Cursors 1 and 2 are indicated in panel A. Cursors 3 and 4 are indicated in panel B. Insets in panels A and B are larger area scans, 60 × 60 $nm^2$, showing the high surface coverage of both systems.**

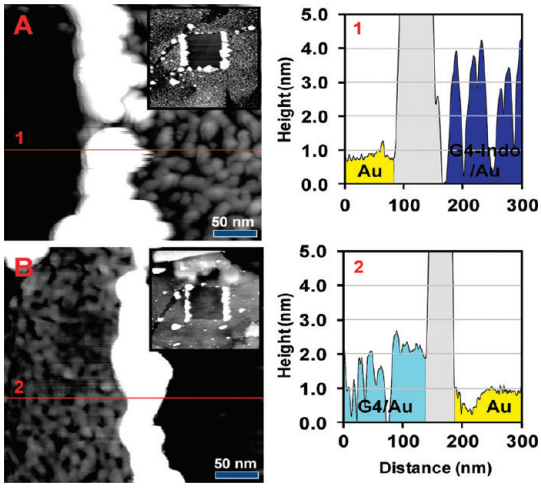


**Figure 2. AFM images of G4 dendrimers with and without indomethacin. (A) A 300 × 300 $nm^2$ AFM topographic image containing bare Au and the G4 PAMAM−OH−$(Pt^{2+})_n$−$(Indo)_m$ dendrimer layer. The (A) inset is a 1.5 × 1.5 $\mu m^2$ AFM topograph of the G4 PAMAM−OH−$(Pt^{2+})_n$−$(Indo)_m$ dendrimer surface where a 500 × 500 $nm^2$ area was removed under high force to expose the Au substrate. Cursor 1 crosses six dendrimers and Au. (B) A 300 × 300 $nm^2$ AFM topograph showing both the G4 PAMAM−OH−$(Pt^{2+})_n$ dendrimer matrix and bare Au surface. The (B) inset is a 1.5 × 1.5 $\mu m^2$ AFM topograph of the G4 PAMAM−OH−$(Pt^{2+})_n$ dendrimer surface where a 500 × 500 $nm^2$ area was removed under high force to expose the Au substrate. Cursor 2 crosses seven G4 dendrimers and a bare Au area.**

which is 0.9 ± 0.1 nm shorter than indomethacin−carrying G4 systems. Bare dendrimers G3−G5 PAMAM−OH−$(Pt^{2+})_n$ follow a different linear correlation,

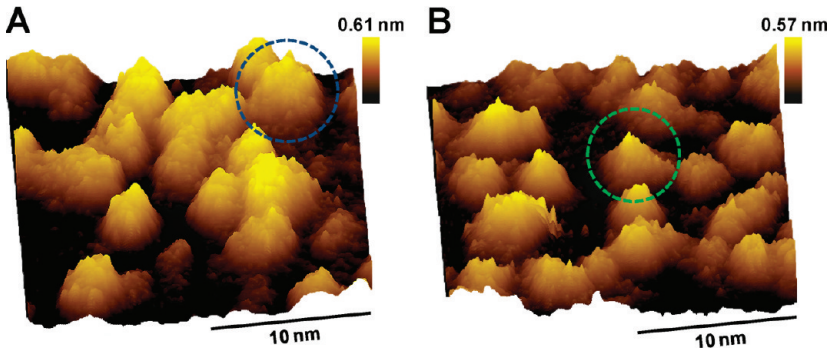


**Figure 3. Indomethacin-loaded dendrimers have a larger volume than unloaded systems of the same generation. (A) A 22 × 22 nm$^2$ STM topograph of G3 PAMAM−OH−$(Pt^{2+})_n$−$(Indo)_m$ dendrimers displayed in 3D. (B) A 22 × 22 nm$^2$ STM topograph of G4 PAMAM−OH−$(Pt^{2+})_n$ dendrimers displayed in 3D. Images were acquired at 0.30 V and 15 pA. The *Z* scale on Figure 3both panels A and B was increased by a factor of 1.5 for the clarity of display.**

**TABLE I. STM Measurements of the Apparent Height ($h_{APP}$), Real Height ($h_{REAL}$), Volume ($V$), and Eccentricity ($\varepsilon$), of G3−G5 Dendrimers with and without Indomethacin**

| dendrimer type | $h_{APP}$ (nm) | $h_{REAL}$ (nm) | $V$ (nm$^3$) | $\varepsilon$ |
|---|---|---|---|---|
| G3 PAMAM−OH−$(Pt^{2+})_n$−$(Indo)_m$ | 0.41 ± 0.08 | 3.2 ± 0.7 | 60 ± 16 | 0.58 ± 0.13 |
| G3 PAMAM−OH−$(Pt^{2+})_n$ | 0.38 ± 0.08 | 2.5 ± 0.3 | 31 ± 7 | 0.56 ± 0.11 |
| G3 PAMAM−OH in solution[12] | N/A | 3.6 | 24 | 0 |
| G4 PAMAM−OH−$(Pt^{2+})_n$−$(Indo)_m$ | 0.57 ± 0.11 | 3.4 ± 0.7 | 72 ± 21 | 0.57 ± 0.13 |
| G4 PAMAM−OH−$(Pt^{2+})_n$ | 0.47 ± 0.07 | 2.5 ± 0.3 | 39 ± 8 | 0.58 ± 0.11 |
| G4 PAMAM−OH in solution[12] | N/A | 4.5 | 47 | 0 |
| G5 PAMAM−OH−$(Pt^{2+})_n$−$(Indo)_m$ | 0.56 ± 0.06 | 3.8 ± 0.7 | 97 ± 14 | 0.58 ± 0.09 |
| G5 PAMAM−OH−$(Pt^{2+})_n$ | 0.51 ± 0.07 | 3.3 ± 0.3 | 68 ± 13 | 0.59 ± 0.13 |
| G5 PAMAM−OH in solution[12] | N/A | 5.4 | 82 | 0 |

$h_{REAL} = 5.11h_{APP} + 0.45$, which is expected as the conductivity of bare dendrimers is higher than the drug-dendrimer complexes.

With the STM apparent height calibrated, the $V$ can be determined from the STM topographs directly because STM exhibits little convolution in the lateral directions. Figure 3 displays a side-by-side comparison of 22 × 22 nm$^2$ STM topographs of G4 dendrimers with (A) and without (B) indomethacin. Assuming an elliptical cap geometry for all dendrimers, the volume of individual molecules may be calculated using: $V = (^1/_6\pi h_{REAL})\text{-}(^3/_4 ab + h_{REAL}{}^2)$, where $a$ and $b$ are the long and short lateral axes, respectively. The lateral dimensions are $a$ = 6.9 nm and $b$ = 6.0 nm for the indomethacin-loaded G4, and the height is 3.3 nm; thus $V$ = 72.5 nm$^3$. From Figure 3B, the unloaded G4 dendrimers measure $a$ = 5.5 nm, $b$ = 5.2 nm, and $h_{REAL}$ = 3.0 nm, which corresponds to a $V$ = 47.8 nm$^3$.

Table I summarizes the $h_{APP}$, $h_{REAL}$, $V$, and $\varepsilon$ values extracted from this investigation. By averaging the measurements of at least 50 dendrimer in each category, the most evident change is the increase in height and volume upon uploading of indomethacin. The eccentricity measurements, $\varepsilon = (1 - b^2/a^2)^{1/2}$, indicate that the lateral deformation of indomethacin-loaded dendrimers is similar to unloaded dendrimers upon being immobilized on surfaces. The similarity in $a$, $b$, and $\varepsilon$ between unloaded and drug−loaded dendrimers indicate that indomethacin binding and surface immobilization do not compromise the integrity and binding of these complexes.

**Visualization of the Hierarchical Structures of Indomethacin Carrying Dendrimers.** The indomethacin is distinctly recognizable in STM topographs because they appear taller and usually broader than the −OH termini of dendrimers. Figure 4 illustrates how to distinguish the two types of features. Figure 4A is an STM topographic image of a G4 PAMAM−OH−$(Pt^{2+})_n$−$(Indo)_m$ dendrimer in which the intramolecular features are clearly visible. At first glance, these intramolecular features exhibit different contrast; that is, some appear brighter than others. Selecting two typical bright and dark features, cursor 1 and 2 indicate the STM apparent height of 0.14 and 0.06 nm, respectively. Both previous and present studies of G4-dendrimer reveal the apparent height of intramoelcular features to be below 0.11 nm.[21] Therefore, we conclude that the bright and tall features identified in Figure 4A are due to the uptake of drugs. To quantify the number of Indomethacin on a surface, we use 0.12 nm as the threshold. Among all 27 intramolecular protrusions visible in Figure 4A, 21 fall under 0.12 nm (0.03 to 0.11 nm), and 6 are above 0.12 nm (0.13 to 0.17 nm), thus 21 termini features and 6 indomethacin molecules. Figure 4B is an STM topographic image of a base dendrimer molecule, G4 PAMAM−OH−$(Pt^{2+})_n$, where intramolecular features, or −OH termini, are clearly visible.[21]

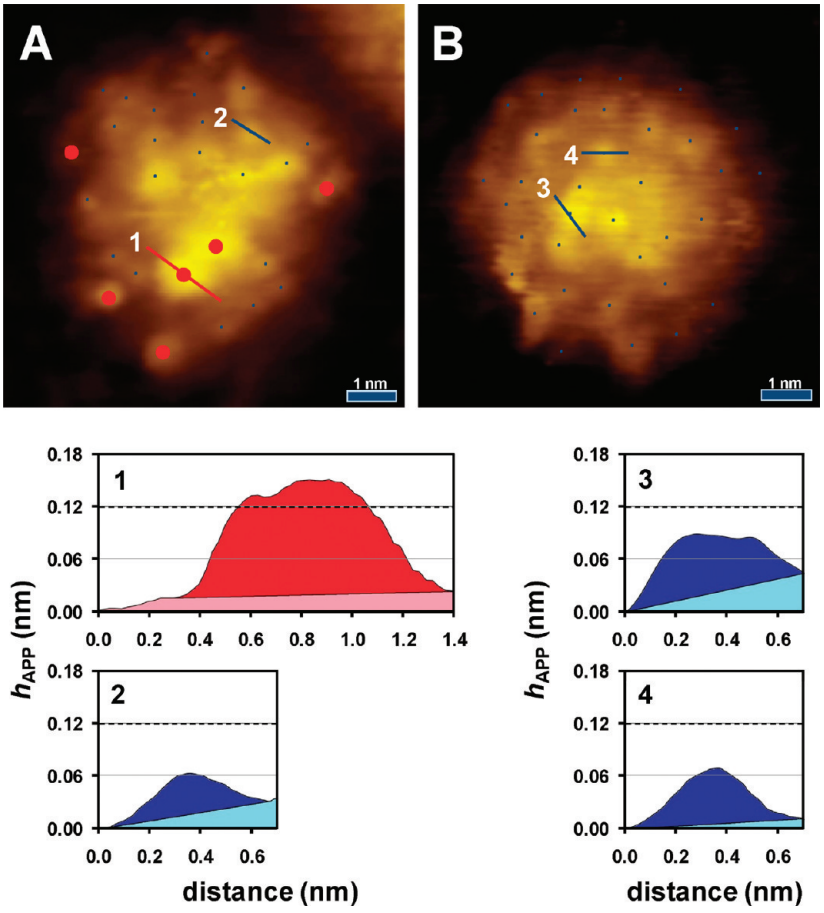


**Figure 4. High-resolution STM images of indomethacin-loaded and unloaded dendrimers. (A) A 6.2 × 6.2 nm$^2$ topographic STM image of a single G4 PAMAM−OH−$(Pt^{2+})_n$−$(Indo)_m$ dendrimer (0.29 V, 21 pA). Red and blue dots mark indomethacin features and hydroxyl termini, respectively. Cursor 1 reveals the dimension of a typical drug feature under STM, while cursor 2 is across a typical dendrimer terminus. (B) A 6.2 × 6.2 nm$^2$ topographic image of a G4 PAMAM−OH−$(Pt^{2+})_n$ dendrimer (0.33 V, 13 pA). Cursor profiles 3 and 4 each bisect a single intramolecular feature from top and middle sites, respectively.**

Cursor profiles 3 and 4 are drawn across two intramolecular features in Figure 4B, accounting for the curvature of the dendrimer molecule. The values of $h_{APP}$ are 0.08 and 0.07 nm, respectively.

Among 20 G4 PAMAM−OH−$(Pt^{2+})_n$−$(Indo)_m$ dendrimers analyzed, indomethacin features have a $h_{APP}$ range = 0.12−0.25 nm with an average $h_{APP}$ = 0.16 nm. In contrast, intramolecular feature $h_{APP}$ measured on indomethacin-loaded and unloaded metal ion-doped G4 PAMAM−OH dendrimers ranged 0.03−0.10 nm, among 40 dendrimers measured previously[21] and in this study. Using the threshold of 0.12 nm, we were able to assign intramolecular and indomethacin features in the STM images. There are six indomethacin on the G4 dendrimer in Figure 4A. The number of indomethacin molecules carried by G4 PAMAM−OH varies from 2 to 14 among the 20 typical dendrimers analyzed. This range is consistent with a previous report where each G4 PAMAM−OH dendrimer molecule held 12.5 indomethacin.[6] It is possible that indomethacin may reside in the dendrimer interior void space, therefore, the observed number of indomethacin per dendrimer most likely represents the minimum uptake. Our investigations indicate that the load increases with generation, for example, G3−G5 PAMAM−OH−$(Pt^{2+})_n$−$(Indo)_m$ dendrimers carry 5−7, 2−14, and 2−19 drugs, respectively.

Based on the $h_{APP}$, and binding strengths (see the next section), the indomethacin may adopt various orientations on the surface of G4. Two likely conformations are shown in Scheme 1. In the case of tall apparent height and relatively weak binding, Scheme 1 uses an example of three H-bonds between the indomethacin's C═O group and the dendrimers' hydroxyl termini. At lower apparent heights and stronger binding, 4 H-bonds are more consistent.

**Indomethacin−Dendrimer Binding Energy As Determined *via* STM Tip Directed Drug Detachment.** Indomethacin on the dendrimer exterior can be removed by the STM tip during scanning. Figure 5A is a high-resolution STM topographical image of a G3 PAMAM−OH−$(Pt^{2+})_n$−$(Indo)_m$ dendrimer obtained at a 0.32 V and 14 pA. Two distinct indomethacin molecules are visible and are labeled 1 and 2. These indomethacin−dendrimer contact areas measure 0.59 and 0.64 nm$^2$ for 1 and 2, respectively. Image 5B was obtained immediately after completion of image 5A. Indomethacin 2, observable in Figure 5A, was

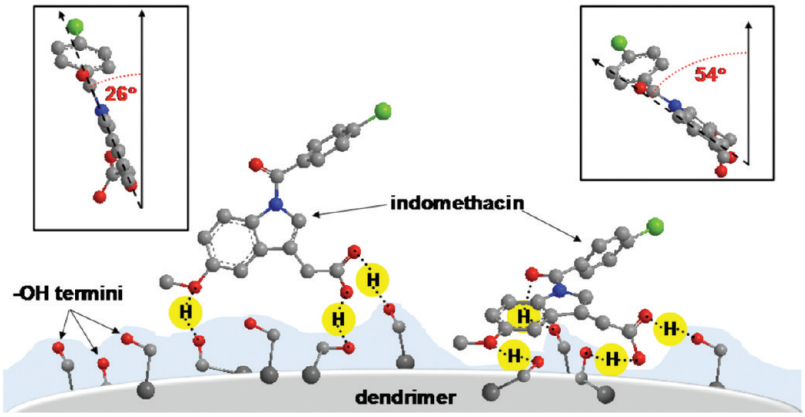


Scheme 1. Possible orientations of indomethacin upon immobilization on dendrimer termini. Indomethacin bound to the dendrimer −OH termini by 3 H-bonds would tilt less than that with 4 H-bonds with respect to surface normal.

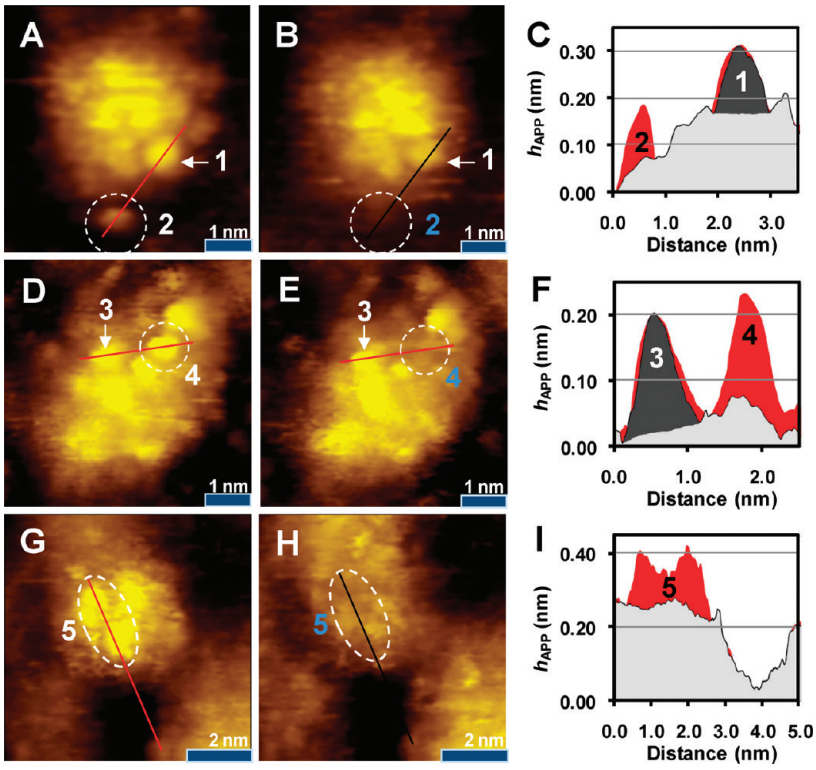


Figure 5. Removal of indomethacin molecules from the surface of dendrimers: (A) 5.7 × 5.7 nm$^2$ STM topograph of a single G3 PAMAM−OH−$(Pt^{2+})_n$−$(Indo)_m$ dendrimer obtained at 0.32 V and 15 pA; (B) same area scanned after panel A, where the indomethacin feature identified in the broken circle disappeared; (C) combined cursor plot for the same line as indicated in panels A and B; (D) 5.6 × 5.6 nm$^2$ STM topograph of a single G4 PAMAM−OH-$(Pt^{2+})_n$-$(Indo)_m$ dendrimer (0.31 V and 22 pA); (E) same area scanned after panel D, where the indomethacin feature identified by the broken circle disappeared; (F) combined cursor plot as indicated in panels D and F; (G) STM topograph of a G5 PAMAM−OH−$(Pt^{2+})_n$−$(Indo)_m$ dendrimer in a 6.2 × 6.2 nm$^2$ scan area obtained at 0.31 V and 18 pA. Two drug features are identified in the broken ellipse; (H) same area scanned in panel G. Both identified indomethacin features were removed; (I) combined cursor plot for the same line in panels G and H.

removed (*i.e.*, missing feature indicated in Figure 5B). The combined cursor plots in Figure 5C, where indomethacin 1 is the landmark, further indicate this removal. The energy from the STM scanning was estimated using[30] $E = eV = 1.6022 \times 10^{-19} \times 0.32 = 5.13 \times 10^{-20}$ (J). The $E$ value represents the maximum energy, assuming a one electron event where all the energy was focused on breaking the indomethacin−dendrimer association. Among 20 removal events, $E$ ranged $4.81-5.29 \times 10^{-20}$ J. In contrast to indomethacin, the characteristic intramolecular features of dendrimer termini remain stable under the same imaging conditions, showing no change for 10+ repetitive scans.

Similar observations were made for G4 PAMAM−OH−$(Pt^{2+})_n$−$(Indo)_m$ as shown in Figure 5D−F. Comparing image 5E to 5D, indomethacin 4 was removed under 0.31 V and 22 pA. Figure 5F is a combined cursor plot, clearly showing the lack of peak 4. The energy

input by the STM probe was $E = 4.97 \times 10^{-20}$ J. The range of $E$ for G4 PAMAM−OH−$(Pt^{2+})_n$−$(Indo)_m$ was $4.81-11.38 \times 10^{-20}$ J over 40 removal events.

In the case of G5 PAMAM−OH−$(Pt^{2+})_n$−$(Indo)_m$ removal occurred at 0.31 V and 18 pA. As shown in Figure 5G two indomethacin molecules are identified within the white dashed ellipse, 5, with contact areas of 0.60 and 0.46 $nm^2$, respectively. In the subsequent scan, Figure 5H, at the same set point both features have been removed. The $E = 4.97 \times 10^{-20}$ J and ranged $4.81-5.29 \times 10^{-20}$ J based on 20 removal events of indomethacin on G5 dendrimers.

To the best of our knowledge, there are no direct measurements of the binding energy between −OH terminated PAMAM dendrimers and molecular NSAIDs to ascertain a direct comparison. Pertaining systems had similar energy values to our STM measurements; for example, the binding energy between amino acid residues in HSA and phenothiazine is between $4.49 \times 10^{-20}$ J and $5.45 \times 10^{-20}$ J as determined by isothermal titration calorimetery.[31] Another measurement is the binding between adenine−thymine dimers, $6.41 \times 10^{-20}$ J as determined *via* the SCC-DFTB method.[32] Our $E$ estimation is also consistent with the H-bond binding energy between the hydroxyl termini of dendrimers and the oxygen and hydroxyl moieties of indomethacin. From the prospective of molecular structure and contact area measurements the −OH and C═O groups of indomethacin could form up to four hydrogen bonds with the −OH termini of dendrimers. H-bonding for one drug molecule to the dendrimer surface could range from $3.49 \times 10^{-20}$ J (one H-bond) to $14.0 \times 10^{-20}$ J (four H-bonds), depending on indomethacin−dendrimer interactions.[13] The energy of removal of indomethacin ranged from $4.81 \times 10^{-20}$ to $11.38 \times 10^{-20}$ J, which is consistent with the breaking of 1−3 H-bonds.

STM-based ambient $I-V$ spectroscopy measurements on individual G4 PAMAM−OH−$(Pt^{2+})_n$−$(Indo)_m$ and G4 PAMAM−OH−$(Pt^{2+})_n$ dendrimers reveal that the addition of indomethacin does not significantly alter the STM electron transport behavior. Figure 6A is a high-resolution STM image of a single G4 PAMAM−OH−$(Pt^{2+})_n$−$(Indo)_m$ dendrimer.

The "×1" is the point where $I-V$ spectroscopy was collected. Figure 6B is a high-resolution STM topograph of an individual G4 PAMAM−OH-$(Pt^{2+})_n$ dendrimer, where $I-V$ spectroscopy was obtained atop the point "×2". Figure 6C contains the $I-V$ curves from ×1 and ×2, respectively. Under the same set point of 0.3 V and 20 pA, curves 1 and 2 are almost identical with the exception of the positive bias region from 0.5 to 1.25 V.

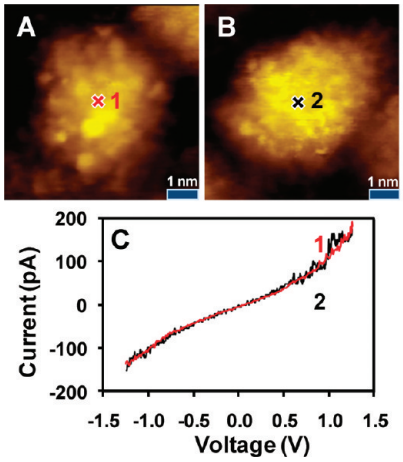


**Figure 6. STM $I-V$ spectroscopy shows that the electron transfer mechanisms for G4 PAMAM−OH−$(Pt^{2+})_n$−$(Indo)_m$ dendrimers and G4 PAMAM−OH−$(Pt^{2+})_n$ dendrimers are similar: (A) 6.1 × 6.1 $nm^2$ STM topographic image of a G4 PAMAM−OH−$(Pt^{2+})_n$−$(Indo)_m$ dendrimer obtained just prior to $I-V$ spectroscopy. The ×1 denotes the lateral STM tip placement for spectroscopic measurement; (B) 7.9 × 7.9 $nm^2$ STM topograph of a G4 PAMAM−OH−$(Pt^{2+})_n$ dendrimer immediately before STM $I-V$ measurement where the ×2 denotes tip placement for spectroscopy; (C) graphical representation of the $I-V$ spectra obtained at points (1) and (2). Both spectra (1 and 2) and images (A and B) were obtained at a set point of 0.30 V and 20 pA.**

Curve 2 (atop the G4 PAMAM−OH−$(Pt^{2+})_n$ dendrimer) displays step features[21] at 0.7 V, 100 pA and 1.0 V, 160 pA. These steps are characteristic of metal ion-doped dendrimers and have been previously reported.[21] Work is in progress to understand the imaging mechanism and the STM electron transport behavior.

## CONCLUSIONS

Using metal ion uptake, this investigation extends STM's high-resolution to reveal the hierarchical structure of indomethacin-loaded PAMAM systems. STM imaging provides structural information about the overall geometry of individual dendrimers such as height, lateral dimensions and volume. In addition, both indomethacin features and dendrimer termini are visualized under the same STM topograph, which enables the identification and count of individual drugs molecules. Removal of drug molecules by the STM tip allows calculation of individual drug-dendrimer binding energy, which is consistent with 1−3 hydrogen bonds. Taken collectively, the binding and resulting conformation of drug and dendrimers may be inferred, which can be used to guide design of new dendrimers for the required stability and delivery performance in the context of dendrimer−based drug delivery vehicles.

## MATERIALS AND METHODS

**Materials.** The 3rd generation PAMAM−OH dendrimer solutions (20% weight in methanol, Sigma-Aldrich), fourth generation PAMAM−OH dendrimer solutions (10% weight in methanol, Sigma-Aldrich), fifth generation PAMAM−OH dendrimer solutions (5% weight in methanol, Sigma-Aldrich), 1-(4-chlorobenzoyl)-5-methoxy-2-methyl-3-indoleacetic acid, commonly

known as indomethacin (≥99.0%, Sigma-Aldrich), and *n*-octanethiol (98%, Sigma-Aldrich), referred to hereafter as $C_8$, were obtained and used without further purification. $K_2PtCl_4$ (min. 42.4% Pt, Alfa Aesar) was used as received. Ultrapure water (≥18 MΩ·cm, Millipore Milli-Q) and 200 proof ethanol (Gold Shield Chemical Co.) were used for dilution and washing. Ultrapure $N_2$ (≥98%, Air Gas Co.) and $H_2$ (99.99%, Praxair, Inc.) were used for drying and flaming, respectively. STM tips were made from W wire ($d$ = 0.010 in., 99.95%, California Fine Wire Co.). For Au thin film preparation, Au slugs (99.99%, Alpha Aesar Premion Co.) and mica (clear ruby muscovite, Mica New York Corp.) were used.

**Preparation of Gold Thin Films.** Au(111) thin films were prepared *via* thermal evaporation of Au onto freshly cleaved mica(0001) in a high-vacuum evaporator (Denton Vacuum, model 502-A).[33] The substrate mica was heated *via* two quartz lamps to 350 °C under a base pressure of $2 \times 10^{-7}$ Torr. The evaporation rate was 0.3 nm/sec and the final thickness of Au films was 150 nm. After evaporation, the Au was thermally annealed *in situ* at 375 °C for 30−60 min to increase the size of the Au(111) terraces. After annealing, the Au film was allowed to cool for ≥5 h under vacuum. Upon removal, the Au films were stored in a sealed glass container and cut and used as needed. Once cut into 1 $cm^2$, the Au films were subjected to $H_2$-flame to remove impurities and to further anneal the surfaces.

**Preparation of Dendrimers on Surfaces for Imaging.** Dendrimer solutions were prepared following previously established procedures.[17,21] In short, PAMAM−OH−$(M^{2+})_n$ dendrimer solutions were made by diluting aliquots of the methanol-based stock solutions to 12.5 μM aqueous solutions. The $K_2PtCl_4$ was then added to the designed molar ratios of 1:20, 1:70, and 1:120 dendrimer/Pt(II) for G3-, G4-, and G5 PAMAM−OH, respectively. After the addition of Pt(II), the final dendrimer concentration was 10 μM. The ratios were selected based on the number of tertiary amines within each dendrimer generation. Pt(II)-doped dendrimers are denoted, for example, G5 PAMAM−OH−$(Pt^{2+})_n$, where $n$ may vary from 0−120 depending on the metal uptake. Once mixed, the solution was kept at room temperature for 3−5 days, allowing sufficient time for Pt(II)−amine coordination within dendrimers.[34] UV−vis spectroscopy (model DU 640i spectrophotometer, Beckman Instruments, Inc.) was employed to monitor metal ion uptake until a steady state was achieved.[35,36] The dendrimer−Pt(II) coordination was monitored *via* absorbance at $\lambda$ = 250 nm,[35] and the maximum intensity was reached and leveled at 48 h and beyond. To attain consistent metal coordination, a minimum of 2.5 days mixing time was allowed for each mixture before deposition on surfaces for STM imaging. In principle, the coordination of $Pt^{2+}$ to amines within dendrimer should not alter the surface −OH termini and there have been less than significant alteration of dendrimer structural integrity from previous investigations.[17]

Indomethacin was weighted and then directly added to the dendrimer solutions in order to obtain 1:20, 1:40, and 1:120 dendrimer/indomethacin molar ratios for G3, G4, and G5 PAMAM−OH−$(Pt^{2+})_n$ dendrimers, respectively. The dendrimer/indomethacin ratio was guided by previous investigations.[5,6] For example, G5 PAMAM−OH−$(Pt^{2+})_n$-indomethacin solutions were prepared by mixing 0.043 g of indomethacin in 100 mL of previously prepared 10 μM G5 PAMAM−OH−$(Pt^{2+})_n$ dendrimer solution. The indomethacin−dendrimer mixture was vortexed for 30 min and allowed to gestate for an additional 2−3 days, with daily 10 min vortexing incorporated.[5] Undissolved indomethacin settled to the bottom of the vial. The clear supernatant was transferred to a new vial. No solids or precipitation were observed after transfer. The final product of indomethacin loaded dendrimers are represented as: G5 PAMAM−OH−$(Pt^{2+})_n$−$(Indo)_m$. Dendrimers remained soluble as $Pt^{2+}$ and indomethacin addition and mixing produced no observable precipitate.

For the surface deposition of dendrimers, 1 $cm^2$ pieces of gold films were $H_2$-flamed,[33] and allowed 20 min cooling under clean ambient conditions. Then, a ∼75.0 μL drop of PAMAM−OH-$(Pt^{2+})_n$-$(Indo)_m$ dendrimer solution was deposited to the Au surface and allowed contact for 1.25 min. The contact diameter of the droplet was typically 0.75 cm. After washing with water and ethanol the surface was exposed to a 1.0 mM $C_8$ solution for 2 min. The formation of $C_8$ SAMs confine dendrimers laterally and prevents mobility during scanning.[21] The surface was then washed again with ethanol and dried under $N_2$ before STM imaging. We recommend highest purity PAMAM for the investigation to minimize the impact of impurities. To avoid contaminants' impact in the process of sample preparation, relatively high concentration is used to yield high coverage of dendrimers on surfaces. For the surface deposition of PAMAM−OH−$(Pt^{2+})_n$ dendrimer solutions, a 125 μL drop was used to obtain the same 0.44 $cm^2$ solution coverage, following the same procedures.

**STM Imaging and Spectroscopy.** The STM has a walker-type scanner (UHV 300, RHK Technologies, Inc.) and was used under ambient conditions for this investigation. The STM tips used for these studies were W wires cut and electrochemically etched at 2.0 V in 3.0 M NaOH solutions. A homemade potentiostat monitored the etching process.[24,33] All STM images were acquired in constant current mode with typical bias voltages ranging from 0.3 to 1.0 V and tunneling currents from 5 to 40 pA. The piezoelectric scanners were calibrated laterally using the decanethiol SAM lattice constant = 0.50 nm and vertically using a Au(111) single atomic step (0.235 nm). Calculation of dendrimer−surface contact area was accomplished using the Image J freeware program (National Institutes of Health, http://rsb.info.nih.gov/ij/).

*I*−*V* measurements were acquired according to the following steps.[24] First, the surface was scanned and individual dendrimer molecules visualized. Second, the scan area was progressively decreased to position the tip above the selected dendrimer, for example, to a 10 × 10 $nm^2$ area. Finally, the current and voltage were typically set to 20 pA and 0.3 V under which an *I*−*V* spectrum was acquired.

**AFM Imaging of Dendrimers.** AFM images were acquired using a MFP3D-SA system (Asylum Research), which includes a closed loop capability. A silicon cantilever (AC-240, Olympus) was used for imaging and nanoshaving.[37] The probe has a force constant of $k$ = 1.0 N/m as measured by thermal noise method.[38] During tapping mode imaging, the cantilever was modulated by a driving frequency of 74 kHz and amplitude of 67.0 nm (0.63 V), with the damping set to 85%. For displacing adsorbates such as dendrimers or alkanethiolates, tips were placed in contact with the surface with increasing load beyond threshold.

*Acknowledgment.* We thank Thomas J. Mullen and Jie-Ren Li at U.C. Davis for many helpful discussions. This work is supported by the University of California, Davis, NSF (CHE 0809977) and an NSF-MRSEC grant through Stanford University's CPIMA program.

## REFERENCES AND NOTES

1. De Jesus, O. L. P.; Ihre, H. R.; Gagne, L.; Frechet, J. M. J.; Szoka, F. C. Polyester Dendritic Systems for Drug Delivery Applications: *In Vitro* and *in Vivo* Evaluation. *Bioconjugate Chem.* **2002,** *13*, 453–461.
2. Henry, C. M. Drug Delivery. *Chem. Eng. News* **2002,** *80*, 39–47.
3. Kaminskas, L. M.; Kota, J.; McLeod, V. M.; Kelly, B. D.; Karellas, P.; Porter, C. J. H. PEGylation of Polylysine Dendrimers Improves Absorption and Lymphatic Targeting Following Sc Administration in Rats. *J. Controlled Release* **2009,** *140*, 108–116.
4. Lee, C. C.; MacKay, J. A.; Frechet, J. M. J.; Szoka, F. C. Designing Dendrimers for Biological Applications. *Nat. Biotechnol.* **2005,** *23*, 1517–1526.
5. Chauhan, A. S.; Jain, N. K.; Diwan, P. V.; Khopade, A. J. Solubility Enhancement of Indomethacin with Poly(Amidoamine) Dendrimers and Targeting to Inflammatory Regions of Arthritic Rats. *J. Drug Target.* **2004,** *12*, 575–583.
6. Chauhan, A. S.; Sridevi, S.; Chalasani, K. B.; Jain, A. K.; Jain, S. K.; Jain, N. K.; Diwan, P. V. Dendrimer-Mediated Transdermal Delivery: Enhanced Bioavailability of Indomethacin. *J. Controlled Release* **2003,** *90*, 335–343.

7. Cheng, Y. Y.; Xu, T. W.; Fu, R. Q. Polyamidoamine Dendrimers Used as Solubility Enhancers of Ketoprofen. *Eur. J. Med. Chem.* **2005,** *40*, 1390–1393.
8. Devarakonda, B.; Hill, R. A.; Liebenberg, W.; Brits, M.; de Villiers, M. M. Comparison of the Aqueous Solubilization of Practically Insoluble Niclosamide by Polyamidoamine (Pamam) Dendrimers and Cyclodextrins. *Int. J. Pharm.* **2005,** *304*, 193–209.
9. Gupta, U.; Agashe, H. B.; Asthana, A.; Jain, N. K. Dendrimers: Novel Polymeric Nanoarchitectures for Solubility Enhancement. *Biomacromolecules* **2006,** *7*, 649–658.
10. Kannan, S.; Kolhe, P.; Raykova, V.; Glibatec, M.; Kannan, R. M.; Lieh-Lai, M.; Bassett, D. Dynamics of Cellular Entry and Drug Delivery by Dendritic Polymers into Human Lung Epithelial Carcinoma Cells. *J. Biomater. Sci., Polym. Ed.* **2004,** *15*, 311–330.
11. Kolhe, P.; Misra, E.; Kannan, R. M.; Kannan, S.; Lieh-Lai, M. Drug Complexation, *in Vitro* Release and Cellular Entry of Dendrimers and Hyperbranched Polymers. *Int. J. Pharm.* **2003,** *259*, 143–160.
12. Man, N.; Cheng, Y. Y.; Xu, T. W.; Ding, Y.; Wang, X. M.; Li, Z. W.; Chen, Z. C.; Huang, G. Y.; Shi, Y. Y.; Longping, W. Dendrimers as Potential Drug Carriers. Part II. Prolonged Delivery of Ketoprofen by *in Vitro* and *in Vivo* Studies. *Eur. J. Med. Chem.* **2006,** *41*, 670–674.
13. Hu, J. J.; Cheng, Y. Y.; Wu, Q. L.; Zhao, L. B.; Xu, T. W. Host−Guest Chemistry of Dendrimer-Drug Complexes. 2. Effects of Molecular Properties of Guests and Surface Functionalities of Dendrimers. *J. Phys. Chem. B* **2009,** *113*, 10650–10659.
14. Nanjwade, B. K.; Bechra, H. M.; Derkar, G. K.; Manvi, F. V.; Nanjwade, V. K. Dendrimers: Emerging Polymers for Drug-Delivery Systems. *Eur. J. Pharm. Sci.* **2009,** *38*, 185–196.
15. Tanis, I.; Karatasos, K. Association of a Weakly Acidic Anti-inflammatory Drug (Ibuprofen) with a Poly(Amidoamine) Dendrimer as Studied by Molecular Dynamics Simulations. *J. Phys. Chem. B* **2009,** *113*, 10984–10993.
16. Zhao, L. B.; Cheng, Y. Y.; Hu, J. J.; Wu, Q. L.; Xu, T. W. Host−Guest Chemistry of Dendrimer−Drug Complexes. 3. Competitive Binding of Multiple Drugs by a Single Dendrimer for Combination Therapy. *J. Phys. Chem. B* **2009,** *113*, 14172–14179.
17. Scott, R. W. J.; Wilson, O. M.; Crooks, R. M. Synthesis, Characterization, and Applications of Dendrimer-Encapsulated Nanoparticles. *J. Phys. Chem. B* **2005,** *109*, 692–704.
18. D'Emanuele, A.; Attwood, D. Dendrimer−Drug Interactions. *Adv. Drug Delivery Rev.* **2005,** *57*, 2147–2162.
19. Binnig, G.; Quate, C. F.; Gerber, C. Atomic Force Microscope. *Phys. Rev. Lett.* **1986,** *56*, 930–933.
20. Binnig, G.; Rohrer, H. Scanning Tunneling Microscopy. *Helv. Phys. Acta* **1982,** *55*, 726–735.
21. Fleming, C. J.; Liu, Y. X.; Deng, Z.; Liu, G. Y. Deformation and Hyperfine Structures of Dendrimers Investigated by Scanning Tunneling Microscopy. *J. Phys. Chem. A* **2009,** *113*, 4168–4174.
22. Nijhuis, C. A.; Oncel, N.; Huskens, J.; Zandvliet, H. J. W.; Ravoo, B. J.; Poelsema, B.; Reinhoudt, D. N. Room-Temperature Single-Electron Tunneling in Dendrimer-Stabilized Gold Nanoparticles Anchored at a Molecular Printboard. *Small* **2006,** *2*, 1422–1426.
23. Scheel, H. J.; Binnig, G.; Rohrer, H. Atomically Flat LPE-Grown Facets Seen by Scanning Tunneling Microscopy. *J. Cryst. Growth* **1982,** *60*, 199–202.
24. Yang, G. H.; Liu, G. Y. New Insights for Self-Assembled Monolayers of Organothiols on Au(111) Revealed by Scanning Tunneling Microscopy. *J. Phys. Chem. B* **2003,** *107*, 8746–8759.
25. Yang, G. H.; Tan, L.; Yang, Y. Y.; Chen, S. W.; Liu, G. Y. Single Electron Tunneling and Manipulation of Nanoparticles on Surfaces at Room Temperature. *Surf. Sci.* **2005,** *589*, 129–138.
26. Tomalia, D. A.; Naylor, A. M.; Goddard, W. A. Starburst Dendrimers—Molecular-Level Control of Size, Shape, Surface-Chemistry, Topology, and Flexibility from Atoms to Macroscopic Matter. *Angew. Chem., Int. Ed. Engl.* **1990,** *29*, 138–175.
27. Eigler, D. M.; Schweizer, E. K. Positioning Single Atoms with a Scanning Tunneling Microscope. *Nature* **1990,** *344*, 524–526.
28. Hamers, R. J.; Tromp, R. M.; Demuth, J. E. Surface Electronic-Structure of Si(111)-(7 × 7) Resolved in Real Space. *Phys. Rev. Lett.* **1986,** *56*, 1972–1975.
29. Riposan, A.; Liu, G. Y. Significance of Local Density of States in the Scanning Tunneling Microscopy Imaging of Alkanethiol Self-Assembled Monolayers. *J. Phys. Chem. B* **2006,** *110*, 23926–23937.
30. Avouris, P.; Walkup, R. E.; Rossi, A. R.; Akpati, H. C.; Nordlander, P.; Shen, T. C.; Abeln, G. C.; Lyding, J. W. Breaking Individual Chemical Bonds *via* STM-Induced Excitations. *Surf. Sci.* **1996,** *363*, 368–377.
31. Cheema, M. A.; Taboada, P.; Barbosa, S.; Castro, E.; Siddiq, M.; Mosquera, V. Energetics and Conformational Changes Upon Complexation of a Phenothiazine Drug with Human Serum Albumin. *Biomacromolecules* **2007,** *8*, 2576–2585.
32. Mamdouh, W.; Dong, M. D.; Xu, S. L.; Rauls, E.; Besenbacher, F. Supramolecular Nanopatterns Self-Assembled by Adenine−Hymine Quartets at the Liquid/Solid Interface. *J. Am. Chem. Soc.* **2006,** *128*, 13305–13311.
33. Riposan, A.; Li, Y.; Tan, Y. H.; Galli, G.; Liu, G. Y. Structural Characterization of Aldehyde-Terminated Self-Assembled Monolayers. *J. Phys. Chem. A* **2007,** *111*, 12727–12739.
34. Pellechia, P. J.; Gao, J. X.; Gu, Y. L.; Ploehn, H. J.; Murphy, C. J. Platinum Ion Uptake by Dendrimers: An NMR and AFM Study. *Inorg. Chem.* **2004,** *43*, 1421–1428.
35. Xie, H.; Gu, Y. L.; Ploehn, H. J. Dendrimer-Mediated Synthesis of Platinum Nanoparticles: New Insights from Dialysis and Atomic Force Microscopy Measurements. *Nanotechnology* **2005,** *16*, S492–S501.
36. Zhao, M. Q.; Sun, L.; Crooks, R. M. Preparation of Cu Nanoclusters within Dendrimer Templates. *J. Am. Chem. Soc.* **1998,** *120*, 4877–4878.
37. Liu, G. Y.; Xu, S.; Qian, Y. L. Nanofabrication of Self-Assembled Monolayers Using Scanning Probe Lithography. *Acc. Chem. Res.* **2000,** *33*, 457–466.
38. Hutter, J. L.; Bechhoefer, J. Calibration of Atomic-Force Microscope Tips. *Rev. Sci. Instrum.* **1993,** *64*, 1868–1873.